JCTC Journal of Chemical Theory and Computation

pubs.acs.org/JCTC Article

Calculation of Excited State Internal Conversion Rate Constant Using the One-Effective Mode Marcus-Jortner-Levich Theory

Aline S. Bozzi* and Willian R. Rocha*

Cite This: J. Chem. Theory Comput. 2023, 19, 2316−2326 Read Online

ACCESS | Metrics & More | Article Recommendations | Supporting Information

ABSTRACT: In this article, the one-effective mode Marcus-Jortner-Levich (MJL) theory and the classical Marcus theory for electron transfer were applied to estimate the internal conversion rate constant, k_{IC}, of organic molecules and a Ru-based complex, all belonging to the Marcus inverted region. For this, the reorganization energy was calculated using the minimum energy conical intersection point to account for more vibrational levels, correcting the density of states. The results showed good agreement with experimental and theoretically determined k_{IC}, with a small overestimation by the Marcus theory. Also, molecules less dependent on the solvent effects, like benzophenone, presented better results than molecules with an expressive dependence, like 1-aminonaphthalene. Moreover, the results suggest that each molecule possesses unique normal modes leading to the excited state deactivation that does not necessarily match the X-H bond stretching, as previously suggested.

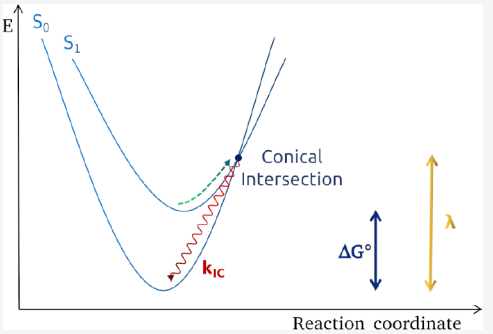

INTRODUCTION

Photophysical processes are of broad interest in many areas of chemistry, physics, and biological sciences. The vast applications encompass environmental science,[1,2] material science,[3] photocatalytic processes,[4−7] solar cells,[8−11] photodynamic therapy,[12−16] and others.[17] Therefore, understanding the photophysical properties that govern the excited state dynamics of such systems is of fundamental interest.

Upon irradiation with a suitable wavelength, a given molecule is excited to higher electronic states, and once there, the deactivation to low-lying energy states begins. Excited state decay mechanisms involve a handful of competing events where two intramolecular deactivation channels are possible: radiative and nonradiative decays, as illustrated in Figure 1. The radiative pathway can occur through fluorescence (F) for a transition between two states of the same spin multiplicity, or through phosphorescence (Ph), for transitions between states with a distinct spin multiplicity. Assuming a closed shell ground state, Kasha's rule[18,19] says that fluorescence always originates from the lowest energy singlet state ($S_1 \rightarrow S_0$), and phosphorescence originates from the lowest energy triplet state ($T_1 \rightarrow S_0$). However, there are examples of violation of this rule in what is called anti-Kasha transitions.[20,21] On the other hand, the nonradiative deactivation process can occur via vibrational relaxation (VR), in which the system geometry relaxes within the same electronic potential energy surface (PES); internal conversion (IC) that, like fluorescence, also happens between states with the same spin multiplicity, while the radiationless decay for different spin states is given through intersystem crossing (ISC) processes. The IC process occurs due to nonadiabatic coupling (NAC) between the states involved in the transition, while the ISC occurs due to spin−orbit coupling.[22,23] Nevertheless, in all cases, the probability of the transition also depends greatly on the energy gap between the states involved.

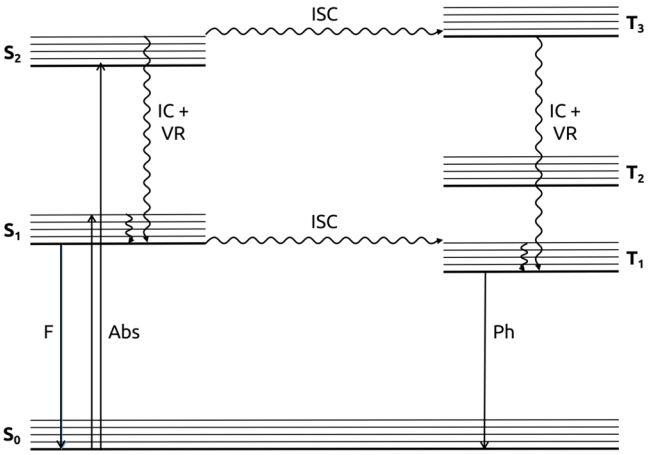

Figure 1. Jablonski diagram.

Received: December 19, 2022
Published: April 6, 2023

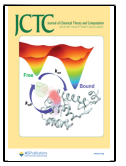

https://doi.org/10.1021/acs.jctc.2c01288
J. Chem. Theory Comput. 2023, 19, 2316−2326

The experimental determination of nonradiative rate constants, k_{nr}, is a difficult task.[24,25] For a small concentration of molecules, the k_{nr} can be approximated by adding the IC and ISC rate constants, k_{IC} and k_{ISC}, respectively, and can be estimated based on the radiative quantum yields (ϕ_f and ϕ_{ph}) and the total radiative rate constant, k_r.[26] The radiative and nonradiative rate constants can also be estimated by *ab inito* calculations.[22] The most popular method for computing radiationless decay rate constants is based on the Fermi Golden Rule, which treats the transition as a time-dependent perturbation.[23] Many authors have applied this method to determine ISC[27−30] and IC[31−33] rate constants. However, the IC rate calculation process is laborious, and several strategies have been implemented, most relying on fitting experimental parameters or on empirical constant values for sets of similar molecules,[34−36] others applying the linear vibronic coupling (LVC) model.[37,38]

In this work, we show that it is possible to use the one-effective mode Marcus-Jortner-Levich (MJL) theory for electron transfer[39] to calculate IC rate constants. We also compare the results with calculations using the semiclassical Marcus' theory,[40−43] a simplified version of the former. Both theories are derived from the Fermi Golden Rule, and, despite its simplicity, Marcus' theory has been applied to ISC rate constant calculations, yielding good results.[27,28,44] It is known that Marcus' theory for electron transfer underestimates rate constant values for molecules within the inverted region, i.e., molecules where the $|\Delta G|$ is greater than the reorganization energy, and the MJL theory overcomes this issue by accounting for the vibronic coupling between the states involved in the transition through a correction to the density of states factor.[45,46] However, the reorganization energy calculation performed classically does not lead to k_{IC} values that agree with the experimentally determined ones. Hence, we propose bypassing this issue by using the minimum energy conical intersection (MECI) between the two transitional states and calculating the reorganization energy at this geometry. This approach assumes the existence of a MECI between the two states and that the mechanism for radiationless deactivation will be given by a change in geometry in the form $S_1 \rightarrow$ MECI $\rightarrow S_0$ going through an activation energy barrier for which no tunneling effects are accounted. Furthermore, the nonadiabatic coupling matrix elements (NACME) are also computed at the MECI geometry since, at this point, the NACME presents its maximum value. Nonetheless, considering that the states are only weakly coupled, and therefore the Fermi Golden Rule can be applied, the nonadiabatic coupling calculated at the S_1 geometry does not significantly change the final rate constant. As we shall see, the procedure is a more direct and cheaper way to compute the internal conversion between two states, giving good results compared with experimental values.

THEORY

Upon absorption of light, the probability, P, of radiationless transition from an initial, $|i\rangle$, to a final, $|f\rangle$, state weakly coupled can be described by a first-order time-dependent perturbation theory as[22,23]

$$P = \frac{2\pi\tau}{\hbar}\langle i|\hat{H}_{if}|f\rangle^2\rho(E) \tag{1}$$

where τ is time, $\hbar$ is the reduced Planck's constant, $\hat{H}_{if}$ is the matrix element of the coupling operator between the two states, and $\rho(E)$ is the density of states per unit of energy. The total transition probability is a linear function of time and, therefore, can be conveniently written as a rate constant,

$$k = \frac{P}{\tau} = \frac{2\pi}{\hbar}\langle i|\hat{H}_{if}|f\rangle^2\rho(E) \tag{2}$$

Equation 2, vastly known as the *Fermi golden rule*,[47] is built upon the assumptions (i) that $\tau \gg [(2\pi\hbar)/(E_f - E_i)]$; and (ii) that both $\hat{H}_{if}$ and $\rho(E_f)$ have a weak dependence toward the final state. For the IC process, the interaction between initial and final states is ruled by the kinetic energy operator, $\hat{T}$, which, under the harmonic approximation, is expressed by[22]

$$\hat{T} = -\sum_j \frac{\hbar\omega_j}{2}\frac{\partial^2}{\partial Q_j} \tag{3}$$

where ω_j and Q_j are the frequency and the dimensionless coordinates associated with the normal mode j, respectively. For the vibronic representation under the adiabatic approximation, the interaction between the initial and final states is given by

$$H_{im,fn} = \left\langle \psi_j^{(f)}\prod_{j=1}^{N}\phi_j^{(fn)}\right| - \sum_j \frac{\hbar\omega_j}{2}\frac{\partial^2}{\partial Q_j}\left|\psi_j^{(i)}\prod_{j=1}^{N}\phi_j^{(im)}\right\rangle \tag{4}$$

Here, the vibronic state is divided into electronic and vibrational contributions. The $\psi_j^{(f)}$ represents the final state electronic wave function at Q_j, while $\prod_{j=1}^{N}\phi_j^{(fn)}$ is the final state vibrational function, which is given as the product of all N vibrational modes, at Q_j with n occupation number for a harmonic potential energy surface (PES) approximation. The same is applicable to the initial state. By dismissing high-order terms for the interaction operator, one gets

$$H_{im,fn} = -\sum_j \hbar\omega_j\left\langle \psi_j^{(f)}\left|\frac{\partial}{\partial Q_j}\right|\psi_j^{(i)}\right\rangle\left\langle \phi_j^{(fn)}\left|\frac{\partial}{\partial Q_j}\right|\phi_j^{(im)}\right\rangle\prod_{\substack{k=1\\k\neq j}}^{N}\langle\phi_k^{(fn)}|\phi_k^{(im)}\rangle \tag{5}$$

where $\hbar\omega_j\left\langle \psi_j^{(f)}\left|\frac{\partial}{\partial Q_j}\right|\psi_j^{(i)}\right\rangle$ is the electronic nonadiabatic coupling (NAC) between the initial and final states for the normal mode j. It has been demonstrated that assuming $m = 0$ is a good approximation for low temperatures[34] and that the other two integrals can be calculated analytically, showing dependence only on n, yielding

$$\left|\langle\phi_j^{(fn)}|\frac{\partial}{\partial Q_j}|\phi_j^{(i0)}\rangle\right|^2 = \frac{1}{2n!}(n - S_j)^2 S_j^{n-1}\exp(-S_j) \tag{6}$$

$$\left|\langle\phi_k^{(fn)}|\phi_k^{(i0)}\rangle\right|^2 = \exp(-S_k)\frac{S_k^n}{n!} \tag{7}$$

where S_j is the Huang−Rhys (HR) factor computed over each normal mode j and can be calculated by projecting the reaction coordinate vectors onto the normal mode coordinate displacement vectors.[48,49] Equation 7 is usually recognized as the Franck−Condon (FC) factor. Under these approaches, eq 2 for the rate constant can be rewritten as

https://doi.org/10.1021/acs.jctc.2c01288
J. Chem. Theory Comput. 2023, 19, 2316−2326

$$k = \frac{2\pi}{\hbar} \sum_{n} \left| \sum_{j} \mathrm{NAC}_j \left\langle \phi_j^{(fn)} \left| \frac{\partial}{\partial Q_j} \right| \phi_j^{(i0)} \right\rangle \prod_{\substack{k=1 \\ k\neq j}}^{N} \langle \phi_k^{(fn)} | \phi_k^{(i0)} \rangle \right|^2 \rho(E) \tag{8}$$

A valid assumption is to consider that the modes inducing the transition (i.e., NAC ≠ 0) and the ones accepting the electronic energy ($S_j \neq 0$) are not the same.[34,50] In this case, eq 6 does not vanish only for $n = 1$ and contributes with $^1/_2$. Also, the density of states is calculated over the energy difference between the two electronic states and corrected by the vibrational levels in the so-called energy-shifted Franck−Condon weighted density (FCWD).[34] The rate equation then becomes

$$k = \frac{\pi}{\hbar} \sum_{\substack{j \\ \mathrm{NAC}_j \neq 0}} |\mathrm{NAC}_j|^2 \sum_{n} \left| \prod_{\substack{k=1 \\ S_k \neq 0}}^{N} \langle \phi_k^{(fn)} | \phi_k^{(i0)} \rangle \right|^2 \rho(E_f - E_i + \sum_k n\hbar\omega_k) \tag{9}$$

Note that, according to eq 9, the rate constant is obtained as summations over all normal modes of the molecule, which imposes limitations for large systems. An alternative procedure would be to perform the calculation only on the normal modes leading to appreciable vibronic coupling, but we usually do not know this information *a priori*.

Another approach to computing the rate constant for radiationless deactivation involving two electronic states is to borrow concepts from the Marcus electron transfer theory. Marcus considered that the vibronic transition scale is considerably smaller than any other vibronic energy scale and, within this semiclassical limit, eq 2 is obtained as[40−43]

$$k_{T,\mathrm{Marcus}} = \frac{2\pi}{\hbar} |\hat{H}_{if}|^2 \frac{1}{\sqrt{\pi\lambda_M k_B T}} \exp\left(\frac{-(\Delta G^\circ + \lambda_M)^2}{4\lambda_M k_B T} \right) \tag{10}$$

where k_B is the Boltzmann's constant, λ_M is the reorganization energy, and ΔG° is the adiabatic energy difference between the relaxed structure of the initial and final electronic states calculated as shown in Figure 2. The reorganization energy, λ_M, is the energy required to relax the structure and the environment upon electron transfer and is computed as the energy difference between the final electronic state in its equilibrium geometry and in the equilibrium geometry of the initial state. Equation 10 is largely applied to electron transfer problems,[44,51−54] but has also been extended to ISC rate constant calculations,[27,28,44] where the coupling matrix element is derived from the spin−orbit coupling (SOC).

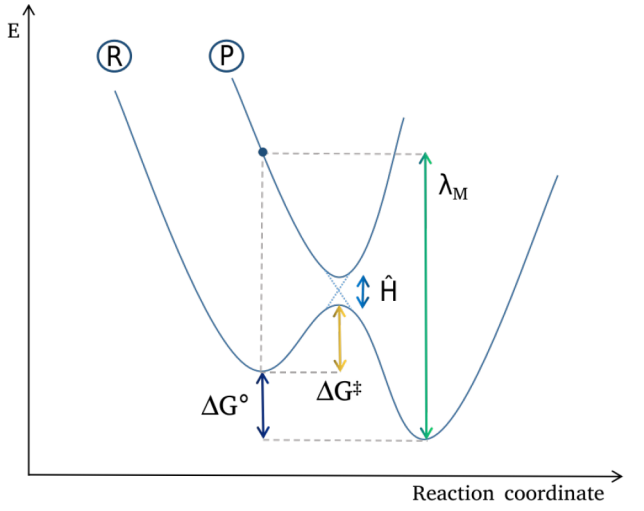

Figure 2. Representation of the coupling between two electronic potential energy surfaces, and the calculations of ΔG° and λ_M.

Usually, the simplified version (eq 10) underestimates the transition rate constant for molecules belonging to the Marcus' inverted region, which is characterized by $-\Delta G^\circ > \lambda_M$ (Figure 3 C).[45,46]

The Marcus-Jortner-Levich (MJL) full-active-space (FAS) theory still considers the semiclassical form for the rate constant. However, it overcomes the deviation from experimental values for the inverted region by accounting for the vibronic coupling between the states, still under the harmonic approximation, and by separating the total reorganization energy into λ_V (inner-sphere) and λ_S (outer-sphere).[39]

$$k_{T,\mathrm{MJL,FAS}} = \frac{\pi}{\hbar} |\mathrm{NAC}|^2 \frac{1}{\sqrt{\pi\lambda_S k_B T}} \exp\left(\sum_{j=1}^{N} -S_j \right) \sum_{n_1=0}^{\infty} \cdots \sum_{n_2=0}^{\infty} \cdots \sum_{n_N=0}^{\infty} \times \left(\prod_{j=1}^{N} \left(\frac{S_j^{n_j}}{n_j!} \right) \exp\left(\frac{-\left(\Delta G^\circ + \lambda_S + \sum_{j=1}^{N} n_j \hbar\omega_j \right)^2}{4\lambda_S k_B T} \right) \right) \tag{11}$$

The similarities between eqs 11 and (9) are apparent. Computing the FAS-based equation is, however, considerably time-consuming as the summations go over the vibrational quantum number, n_j, of each vibrational mode, j, and, therefore, its computational cost increases drastically for larger molecules. Nonetheless, it has been demonstrated by Closs et al. that approximating the FAS theory by a one-effective mode yields good results.[55,56] In fact, many authors have been using this approach in miscellaneous problems involving charge transfer and photoinduced processes.[57−59] Therefore, the one-effective mode equation reads

$$k_{T,\mathrm{MJL,eff}} = \frac{\pi}{\hbar} |\mathrm{NAC}|^2 \frac{1}{\sqrt{\pi\lambda_M k_B T}} \sum_{n=0}^{\infty} \exp(-S) \frac{S^n}{n!} \exp\left(\frac{-(\Delta G^\circ + \lambda_M + n\hbar\omega_{\mathrm{eff}})^2}{4\lambda_M k_B T} \right) \tag{12}$$

where S is the summation over all S_j and ω_{eff} is calculated based on the HR factors as,

$$\omega_{\mathrm{eff}} = \frac{\sum_{j=1}^{N} S_j \omega_j}{\sum_{j=1}^{N} S_j} \tag{13}$$

In this work, we show that, by extending the Fermi golden rule under the one-effective mode MJL approximation, it is possible to calculate the IC rate constants in good agreement with previous theoretical works and experimental data. Furthermore, we also demonstrate that to do so, the reorganization energy has to be calculated regarding the minimum energy conical intersection involving the initial and final states (Figure 3 C). The reorganization energy calculated regarding the MECI geometry imposes a correction to the whole density of states factor rather than just the reorganization energy itself, and so eq 12 is rewritten as

https://doi.org/10.1021/acs.jctc.2c01288
J. Chem. Theory Comput. 2023, 19, 2316−2326

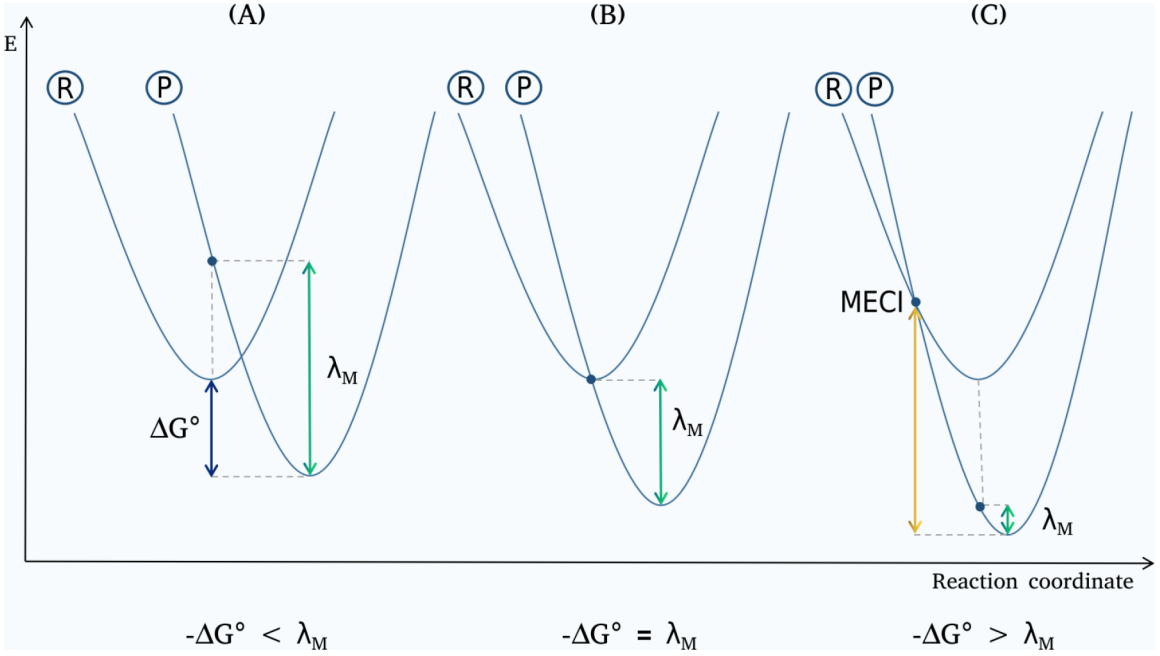

Figure 3. Reorganization energy for different Marcus regions: (A) the normal region, where $-\Delta G^\circ < \lambda_M$; (B) the region where $-\Delta G^\circ = \lambda_M$; and (C) the inverted region, where $-\Delta G^\circ > \lambda_M$.

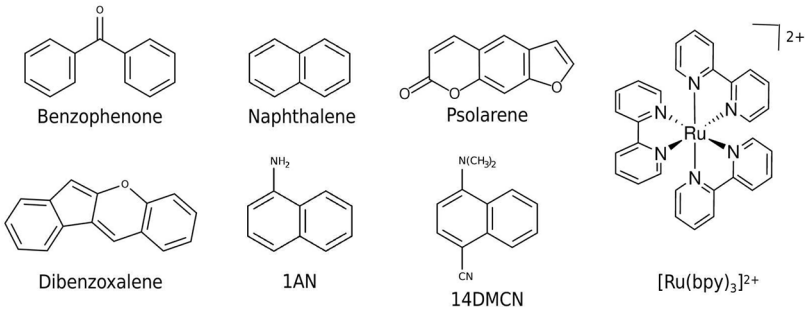

Figure 4. Set of Marcus inverted region molecules for the IC rate constant calculation in this work.

$$k_{IC} = \frac{\pi}{\hbar}|\mathrm{NAC}|^2 \frac{1}{\sqrt{\pi\lambda_{MECI}k_B T}} \sum_{n=0}^{\infty} \exp(-S)\frac{S^n}{n!} \exp\left(\frac{-(\Delta G^\circ + \lambda_{MECI} + n\hbar\omega_{eff})^2}{4\lambda_{MECI}k_B T}\right) \quad (14)$$

Here, only the inner-sphere reorganization energy is calculated, which is given as the difference between the minimum energy conical intersection energy and the minimum PES energy of the final state, and the NAC is computed at the MECI geometry.

METHODS

In order to test the validity of this approach, we considered the molecules illustrated in Figure 4. The set of molecules includes benzophenone, naphthalene, psolarene, dibenzoxalene, 1-aminonaphthalene (1AN), 1-dimethylamino-4-cyanonaphthalene (14DMCN), and Tris(2,2′-bipyridine)ruthenium(II). Besides having their photophysics largely described by both experimental and theoretical works,[22,31,34,36,60−65] their shared characteristic is the aromatic moiety, which carries an expressive rigidity when compared to others. This rigidity is responsible for the small change in geometry between different states PES, culminating in a small reorganization energy, λ_M. Therefore, these molecules are grouped in the Marcus inverted region. The main electronic transition for the set of organic molecules involves the first singlet excited state ($S_1 \rightarrow S_0$), which is essentially $\pi \rightarrow \pi^*$ in nature and, therefore, these two states were chosen for the internal conversion study reported here. It is worth mentioning that, however, benzophenone is an exception to this, and its photophysics can also proceed involving the $n \rightarrow \pi^*$ state or even through a three-state quasi-degeneracy region involving both singlet and triplet manifolds.[31] In our calculations, the transition is represented by both $n \rightarrow \pi^*/\pi \rightarrow \pi^*$, meaning major and minor contributions, respectively. For the $[Ru(bpy)_3]^{2+}$, the S_1 state is MLCT (metal−ligand charge transfer) in nature. The first triplet state of the molecules was also investigated.

Full unconstrained geometry optimizations and frequency calculations for states S_0, S_1, and T_1 for all molecules were carried out using the ORCA-5.0.3 software.[66,67] Density Functional Theory (DFT), both time-dependent and independent, was used with the hybrid functional B3LYP.[68] The Ahlrichs full-electron def2-TZVP(-f) basis set[69] was used for all atoms, and the calculations included the Grimme's D3 dispersion correction[70] with the Becke-Johnson (BJ) damping.[71] Coulomb integrals were sped up by RI approximation[72] using def2/J as an auxiliary basis set.[73] The Tamm-Dancoff approximation (TDA)[74] was used to calculate the excited state. The

https://doi.org/10.1021/acs.jctc.2c01288
J. Chem. Theory Comput. 2023, 19, 2316−2326

conductor-like polarizable continuum model (C-PCM)[75] was used to perform all calculations for the $[Ru(bpy)_3]^{2+}$ complex to simulate water solvation. For this case linear response (LR-CPCM) formalism[76] was used for both geometry optimization and excitation energies within the equilibrium and non-equilibrium regimes, respectively. The properties of the organic molecules were calculated in the gas phase. The free energies, $\Delta G°$, of all molecules, were calculated as shown in Figure 2, as the adiabatic energy difference between the equilibrium geometries of S_0 and S_1 states.

The classical Marcus reorganization energies, λ_M, were calculated in order to check whether the molecules were grouped in the Marcus inverted region. Single point energy calculations were performed for the S_0 state at the S_1 equilibrium geometry ($S_0@S_1$) at the B3LYP/def2-TZVP(-f) level of theory. Then, λ_M was determined as the energy difference in the S_0 PES at S_1 and S_0 equilibrium geometries, given as

$$\lambda_M = S_0@S_1 - S_0@S_0 \tag{15}$$

which considers only the inner-sphere contribution.[77−80]

The minimum energy conical intersection reorganization energies, λ_{MECI}, proposed in this work, were calculated as follows,

$$\lambda_{MECI} = E_{MECI} - S_0@S_0 \tag{16}$$

where E_{MECI} is the energy computed at the minimum energy conical intersection geometry between the S_0 and S_1 states. The idea is that, when computing the reorganization energy at this point of maximum nonadiabatic coupling, a correction to the whole density of states factor (eq 14) is imposed, rather than just on the reorganization energy itself. This reorganization energy can be considered as the amount of energy necessary to relax the structure to the final S_0 state from the minimum energy conical intersection point. Although TDDFT can be used to determine the minimum energy conical intersection between two PES, it might predict the wrong dimensionality for the intersection space. In this case, the spin-flip TDDFT (SF-TDDFT)[81] method is advised, which uses the T_1 state as the reference state, and calculates both the S_0 and S_1 as excited states. The method of the gradient projection (GP)[82] was used to find the minimum energy conical intersection point. Once the MECI geometries and the λ_{MECI} were determined, the NAC was calculated between the ground state and the first singlet excited state[83] at the MECI geometry for each molecule.

To determine the HR factor for each molecule, we used the Dushin code.[49] To do so, we calculated the S_0 and S_1 normal-mode frequencies at their respective equilibrium geometries at B3LYP/6-31G* level of theory for the organic molecules and the bpy ligand of the complex, while the Ru was treated with LANL2DZ and the pseudopotential[84] using the Gaussian 09 software.[85]

The k_{IC} was computed using a FORTRAN95-built code. Although it is a very simple and straightforward calculation, we are open to sharing the code with the community. It can be downloaded at https://ecsmolab.qui.ufmg.br.

RESULTS AND DISCUSSION

Free Energies and Frequencies. The free energies of all molecules were calculated as the adiabatic energy difference between the equilibrium geometries of the S_0 and S_1 states and are shown in Table 1. As expected, the $\Delta G°$ values are negative, considering that the initial states are higher in energy than the final states. Table 1 also shows the Marcus reorganization energy values calculated using eq 15, which are considerably lower than their corresponding free energy moduli. This indicates that the molecules are, in fact, located at the Marcus inverted region.

Table 1. Calculated $\Delta G°$ and λ_M for Each Molecule

Molecule	$\Delta G°$ (eV)	λ_M (eV)
Benzophenone	−3.295	0.395
Naphthalene	−4.375	0.104
Dibenzoxalene	−2.095	0.555
Psolarene	−3.477	0.460
1AN	−3.656	0.321
14DMCN	−2.909	0.639
$[Ru(bpy)_3]^{2+}$	−2.303	0.198

Huang-Rhys Factor and Effective Frequency. The total HR factors and effective frequencies for the set of molecules are shown in Table 2. The effective frequency has an expressive dependence on the HR factor, as demonstrated in eq 13, and only values of $S_j \geq 0.03$ were considered representative, as discussed before by Chaudhuri et al.,[45] meaning these are the normal modes that contribute most to the transition by accepting the electronic energy, especially for molecules of the Marcus inverted region.

Table 2. Calculated HR Factors and Effective Frequencies for Each Molecule

Molecule	HR Factor	$\tilde{\omega}_{eff}$ (cm^{-1})
Benzophenone	2.296	1539.6
Naphthalene	0.828	844.9
Dibenzoxalene	5.155	540.9
Psolarene	4.764	502.3
1AN	4.197	284.2
14DMCN	55.531	137.4
$[Ru(bpy)_3]^{2+}$	2.769	314.5

The effective frequencies range from 1539.6 to 137.4 cm^{-1}, which is far from the characteristic frequencies of the C−H bond displacements for organic molecules, suggested to be responsible for the radiationless deactivation of the excited states.[63,86−88]

Besides the HR factor and the effective frequency, the occupation number also reflects on the IC rate constant. Small values of S_j are associated with a major contribution from $n = 0$, while larger values of S_j have more contributions from other excited vibrational levels. This tendency can be observed in Figure 5, which shows the convergence of the FCWD factor as a function of n. All molecules but 14DMCN show full convergence at $n < 15$, which agrees with a small total HR factor (<6), naphthalene being the molecule with the lowest HR factor and the fastest convergence. On the other hand, 14DMCN converged for $n > 65$, showing an expressively high HR factor of 55.531.

Minimum Energy Conical Intersection, Reorganization Energy, and Nonadiabatic Couplings. The Marcus inverted region is majorly composed of molecules containing rigid moieties. Hence, their equilibrium geometries for ground and excited states are virtually the same, showing minimal differences. Consequently, the classical reorganization energy can be considerably lower than the free energy, and the density of states can be compromised. Instead, by considering that the transition will follow the mechanism $S_1 \rightarrow$ MECI $\rightarrow S_0$ and will not deactivate by tunneling, the density of states can be

https://doi.org/10.1021/acs.jctc.2c01288
J. Chem. Theory Comput. 2023, 19, 2316−2326

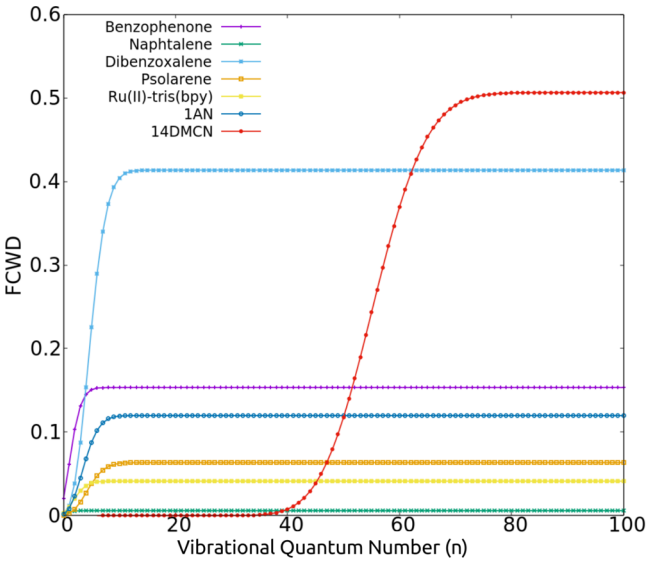

Figure 5. Convergence of the FCWD given as a function of the vibrational quantum number.

corrected by using the minimum energy conical intersection point between the two states involved in the transition. As shown in Figure 6, the ground and first excited singlet states present almost identical equilibrium geometries. The only molecule showing worth-mentioning change is 14DMCN, for which the S_1 geometry presents a tilt on the amine group compared to the S_0 geometry. Contrasting, the MECIs present significant changes in their geometries. Interestingly, these changes show minor contributions from C−H bond stretching, meaning other normal modes can induce the decay.

Benzophenone, as previously demonstrated, has a small difference in the C═O bond length, and the angle between the two aromatic rings for states S_0 and S_1 (1.23 Å and 50°; 1.32 Å and 40°, respectively),[31] which was reproduced in our calculations (1.219 Å and 55.28°; 1.315 Å and 40.23°, respectively), while the minimum energy conical intersection geometry shows a C═O bond length of 1.627 Å and dihedral angle between the rings of 0.112°. The C═O bond stretching occurs for normal modes between 1282.7 and 1612.6 cm^{-1}, a frequency range that comprises the effective frequency calculated for this molecule, suggesting these are the modes most contributing to the internal conversion.

Naphthalene, 1AN, and 14DMCN share the same framework composed of two rings forming an aromatic moiety and, therefore, present similar distortions for the minimum energy conical intersection geometry. The change is observed as a torsion of the ring possessing substituent groups for 1AN and 14DMCN. Such a difference is not noticed between the equilibrium geometry of states S_0 and S_1 of the molecules. Although geometry distortions are similar, each molecule's effective frequency differs significantly. Nonetheless, all the effective frequencies correspond to normal modes where hydrogens or the CN group, for the 14DMCN, bounce off of the ring plane, implying a distortion on that ring. The frequency values differ due to different groups binding to the framework, which will affect bond strength and length.

For dibenzoxalene, a molecule even more rigid, the conformational change toward the minimum energy conical intersection appears as bond length stretching, which occurs at the five-membered ring, where the minimum energy conical intersection geometry shows a C−C bond length of 1.575 Å neighboring the oxygen-containing ring. For the S_0 and the S_1 states, the same bond has lengths of 1.354 and 1.438 Å, respectively. The effective frequency of 540.9 cm^{-1} for this molecule corresponds to angular distortions of the five-membered ring; however, the referenced bond stretching occurs at 1641.8 cm^{-1}.

Although psoralene also possesses a rigid framework like dibenzoxalene, its minimum energy conical intersection geometry shows an off-plane distortion where the two hydrogens of the lactone ring form a dihedral angle of 85.31°. Such distortion is partially given by a normal mode at 535.3 cm^{-1}, which is considerably close to the calculated effective frequency.

The $[Ru(bpy)_3]^{2+}$ is a more complex molecule containing a metal center. Nevertheless, besides its complexity, the bipyridine ligand is aromatic, a characteristic of all molecules presented here. This feature allocates this metal complex at the inverted region and shows very restricted changes, being the most pronounced effect a small twist on the ligands, which are no longer with their rings aligned. Such distortion is seen in several normal modes, all below 730 cm^{-1}, where some are below, and others are above the effective frequency calculated (314.5 cm^{-1}).

Table 3 shows the corrected reorganization energy calculated regarding the minimum energy conical intersection point for each molecule. The λ_{MECI} energy is up to ten times greater than the classical reorganization energy, being closer to the free energy values. However, it is not responsible for correcting the FCWD factor alone, as the density of states is also corrected by the HR factor and the introduction of an effective frequency. The effect will be clearer in the next section.

It is also interesting to note that even though the nonadiabatic couplings between the S_1 and S_0 states were calculated at the minimum energy conical intersection geometries, the coupling values were low, indicating that the states are weakly coupled, and the Fermi Golden Rule is applicable.

Internal Conversion Rate Constant. Table 4 shows the experimental IC rate constants for the set of molecules. It also shows k_{IC} calculated in previous works, and the results calculated using the one-effective mode MJL and the classical Marcus equation, using the λ_{MECI}. At first glance, it is noticeable that the IC rate constants calculated by the one-effective mode MJL theory are consistent and agree with the experimental values, with few discrepancies. Furthermore, the semiclassical Marcus equation also yielded good results but presented a larger deviation from experimental values.

Although all molecules but $[Ru(bpy)_3]^{2+}$ were calculated using gas-phase, the agreement with experimentally determined values varied. Benzophenone and naphthalene presented the closest results between the experimentally determined and the calculated through one-effective mode MJL k_{IC}. The experimental results for benzophenone were obtained in liquid paraffin.[60] However, Marazzi et al. demonstrated that the solvent nature does not affect the qualitative and semiquantitative optical properties of this molecule,[90] which has been confirmed by Shizu and Kaji.[31] For naphthalene, the experimental k_{IC} was estimated by Valiev et al. using the experimental fluorescence lifetime and quantum yield values.[63,89] Although the experiments were performed in cyclohexane, the theoretical constant value calculated in the gas phase also agrees with it, suggesting that the solvent does not play an important role in the photophysics of the molecule. In fact, both the cyclohexane and

https://doi.org/10.1021/acs.jctc.2c01288
J. Chem. Theory Comput. 2023, 19, 2316−2326

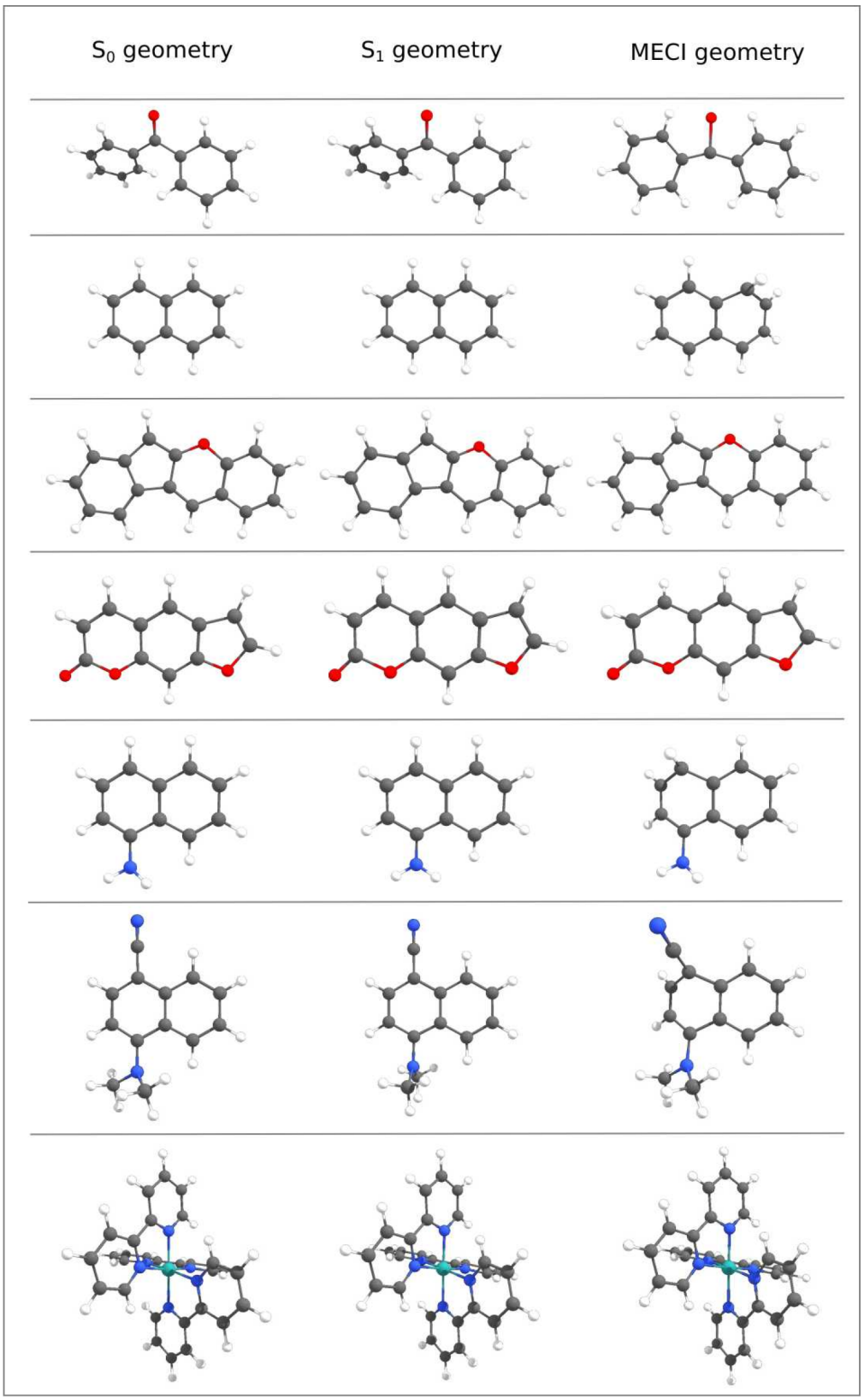

Figure 6. Equilibrium geometries of states S_0 and S_1 and minimum energy conical intersection geometry of benzophenone, naphthalene, dibenzoxalene, psoralene, 1AN, 14DMCN, and $[Ru(bpy)_3]^{2+}$, respectively.

liquid paraffin are apolar solvents and are expected to interact with the medium weakly.

On the other hand, dibenzoxalene is the molecule that presented the worst agreement between the experiments and the calculations. However, it is interesting mentioning that the value presented in Table 4 refers to the total experimental non-radiative rate constant, k_{nr}, which accounts for both k_{IC} and k_{ISC}, as previously mentioned. In this case, it is expected for the k_{IC} to

https://doi.org/10.1021/acs.jctc.2c01288
J. Chem. Theory Comput. 2023, 19, 2316−2326

Table 3. Calculated λ_{MECI} and |NAC| for Each Molecule

Molecule	λ_{MECI} (eV)	|NAC| (cm^{-1})
Benzophenone	4.189	0.40
Naphthalene	3.099	0.46
Dibenzoxalene	1.707	2.06
Psolarene	2.621	0.88
1AN	2.868	0.63
14DMCN	2.503	0.66
$[Ru(bpy)_3]^{2+}$	3.348	1.00

be lower than the total nonradiative constant. Furthermore, Valiev et al. calculations also predicted a considerably lower internal conversion rate constant,[63] suggesting our estimations are consistent. Besides, it is possible that the dibenzoxalene photophysical properties are more dependent on the solvent nature, even though the experiments were reported to be performed in cyclohexane.

The dependence on the solvent nature is well illustrated for the 1AN and 14DMCN molecules, and the reported experimental rate constants in Table 4 refer to acetonitrile as the solvent. However, the authors also reported rate constants determined in hexane and diethyl ether, resulting in different k_{IC} values. For 1AN and 14DMCN the $\log(k_{IC})$ in hexane was 7.14 s^{-1} and 11.24 s^{-1}, respectively, while in diethyl ether the values were 7,04 s^{-1} and 9,72 s^{-1}, respectively.[64] While our calculations performed in gas-phase are closer to the experimental values performed in acetonitrile, the calculated values by Kohn et al., also presented in Table 4, are considerably higher, especially for 14DMCN, which agrees with experimental values performed on hexane.[36,64] Nonetheless, their work does not mention whether the calculations considered any solvation method.

The estimated IC rate constant of psoralene was higher than the one previously calculated by Valiev et al.[63] The authors made systematic comparisons with other coumarins[91] and evaluated the consistency of their methods based on experimental fluorescence and quantum yields. The solvation methods were not explicitly mentioned.

Similarly to dibenzoxalene, the $[Ru(bpy)_3]^{2+}$ experimentally determined rate constant was also given in terms of the total nonradiative decay in water.[65] Although our calculations used implicit solvation to simulate the environment, the k_{IC} value was higher than the experimental k_{nr} for both methods. Ruthenium complexes with nitrogen-containing conjugated ligands are known for their high performance as photosensitizers,[92] which are characterized by a strong spin−orbit coupling between excited singlet−triplet states, which is translated into high k_{ISC}. It suggests that even though the k_{IC} calculated for this compound is close to the k_{nr}, the methods hereby used overestimate the rate constant value.

As an overall result, the classical Marcus theory predicted higher rate constants compared to the one-effective mode MJL, which is the opposite of expected since the MJL proposition was to avoid underestimations for the inverted region. However, it is wise to keep in mind that these formulations were originally proposed for electron-transfer problems.

CONCLUSIONS

In this work, we have applied the classical Marcus theory and the one-effective mode MJL theory for electron transfer to calculate the internal conversion rate constant of $S_1 \rightarrow S_0$ deactivation of a set of molecules of the inverted region. To do so, we incorporated a correction to the density of states by using the minimum energy conical intersection energies to determine the new reorganization energy. In general, both theories yielded good results that are in agreement with the experimental rate constants of each molecule, although the Marcus theory presented a higher overestimation for k_{IC}. Besides, the results were comparable to previously calculated rate constants computed with a handful of methods already described.

These results showed that the use of minimum energy conical intersection energies on the reorganization energy is a good estimation to correct the density of states. Furthermore, the HR factor and the effective frequencies also contributed to refining the corrections. It was seen that each molecule has a unique effective frequency that corresponds to a combination of normal modes that does not necessarily match the X-H bond stretching, as previously suggested.

ASSOCIATED CONTENT

Supporting Information

The Supporting Information is available free of charge at https://pubs.acs.org/doi/10.1021/acs.jctc.2c01288.

The coordinates of equilibrium geometries of states S_0 and S_1 and for the minimum energy conical intersection of all molecules (PDF)

AUTHOR INFORMATION

Corresponding Authors

Aline S. Bozzi − *Laboratório de Estudos Computacionais em Sistemas Moleculares, eCsMolab, Departamento de Química, ICEx, Universidade Federal de Minas Gerais, 31270-901 Belo Horizonte, MG, Brazil*; Email: alinebozzi@qui.grad.ufmg.br

Willian R. Rocha − *Laboratório de Estudos Computacionais em Sistemas Moleculares, eCsMolab, Departamento de Química, ICEx, Universidade Federal de Minas Gerais, 31270-901 Belo Horizonte, MG, Brazil*; orcid.org/0000-0002-0025-2158; Phone: +55 (31) 3409-5776; Email: wrocha@ufmg.br

Table 4. Experimental and Theoretical Determination of the IC Rate Constant for Each Molecule

Molecule	$\log(k_{IC}^{exp}/s^{-1})$	$\log(k_{IC}^{calc}/s^{-1})^a$	$\log(k_{IC}^{calc}/s^{-1})^b$	$\log(k_{IC}^{calc}/s^{-1})^c$
Benzophenone	<7[22,60]	6.55[31]	6.50	7.20
Naphthalene	5.30[63,89]	−4.21[34]	5.27	5.91
Dibenzoxalene	11.89[34,62]	9.66[34]	8.54	8.53
Psolarene	-	5.70[63]	6.89	7.27
1AN	6.30[64]	7.39[36]	6.87	7.37
14DMCN	8.55[64]	10.92[36]	7.57	8.06
$[Ru(bpy)_3]^{2+}$	6.12[65]	-	6.76	7.07

[a]Calculated in other works. [b]Calculated in this work using the one-effective mode MJL theory. [c]Calculated in this work using the classical Marcus theory.

https://doi.org/10.1021/acs.jctc.2c01288
J. Chem. Theory Comput. 2023, 19, 2316−2326

Complete contact information is available at:
https://pubs.acs.org/10.1021/acs.jctc.2c01288

Notes

The authors declare no competing financial interest.

■ ACKNOWLEDGMENTS

The authors thank CNPq (Conselho Nacional de Desenvolvimento Científico e Tecnológico, INCT-Catálise), CAPES (Comissão de Aperfeiçoamento Pessoal), and FAPEMIG (Fundação de Amparo à Pesquisa do Estado de Minas Gerais) for the financial support. The authors also acknowledge the free-of-charge availability of the ORCA package for academic purposes.

■ REFERENCES

(1) Vione, D. Photochemical Transformation Processes of Environmental Significance. *Tomorrow's Chemistry Today* **2008**, 429−453.
(2) Sleiman, M.; Nienow, A.; Richard, C. Environmental photochemistry on plants: recent advances and new opportunities for interdisciplinary research. *Photochemical and Photobiological Sciences* **2022**, *21*, 1497−1510.
(3) Setoura, K.; Ito, S. Optical manipulation in conjunction with photochemical/photothermal responses of materials. *Journal of Photochemistry and Photobiology C: Photochemistry Reviews* **2022**, *52*, 100536.
(4) Takeda, H.; Koike, K.; Morimoto, T.; Inumaru, H.; Ishitani, O. Photochemistry and photocatalysis of rhenium(I) diimine complexes. *Adv. Inorg. Chem.* **2011**, *63*, 137−186.
(5) Yawalkar, A. A.; Bhatkhande, D. S.; Pangarkar, V. G.; Beenackers, A. A. Solar-assisted photochemical and photocatalytic degradation of phenol. *J. Chem. Technol. Biotechnol.* **2001**, *76*, 363−370.
(6) Yoon, T. P.; Ischay, M. A.; Du, J. Visible light photocatalysis as a greener approach to photochemical synthesis. *Nat. Chem.* **2010**, *2*, 527−532.
(7) Weerasooriya, R. B.; Drummer, M. C.; Phelan, B. T.; Gesiorski, J. L.; Sprague-Klein, E. A.; Chen, L. X.; Glusac, K. D. Toward Metal-free Photocatalysis: Photochemical Regeneration of Organic Hydride Donors Using Phenazine-Based Photosensitizers. *J. Phys. Chem. C* **2022**, *126*, 17816−17825.
(8) Cheng, Y. Y.; Fückel, B.; MacQueen, R. W.; Khoury, T.; Clady, R. G.; Schulze, T. F.; Ekins-Daukes, N. J.; Crossley, M. J.; Stannowski, B.; Lips, K.; Schmidt, T. W. Improving the light-harvesting of amorphous silicon solar cells with photochemical upconversion. *Energy Environ. Sci.* **2012**, *5*, 6953−6959.
(9) Ling, T.; Kulinich, S. A.; Zhu, Z. L.; Qiao, S. Z.; Du, X. W. Highly Conductive CdS Inverse Opals for Photochemical Solar Cells. *Adv. Funct. Mater.* **2014**, *24*, 707−715.
(10) Nastasi, F.; Mineo, P. G.; Barichello, J.; La Ganga, G.; Di Marco, G.; Calogero, G.; Cordaro, M. Synthesis and Photophysics Characterization of Boronic Styril and Distyryl BODIPYs for Water-Based Dye-Sensitized Solar Cells. *Biomimetics* **2022**, *7*, 110.
(11) Shen, F.; Fan, Y. M.; Li, H.; Li, S. P.; Xu, M.; Dai, W. B. Photophysics and photovoltaic properties of Zn-alloyed Ag-In-S quantum dots sensitized solar cells. *J. Alloys Compd.* **2022**, *922*, 166296.
(12) Tavakoli, A.; Min, J. H. Photochemical modifications for DNA/RNA oligonucleotides. *RSC Adv.* **2022**, *12*, 6484−6507.
(13) Rickard, B. P.; Overchuk, M.; Obaid, G.; Ruhi, M. K.; Demirci, U.; Fenton, S. E.; Santos, J. H.; Kessel, D.; Rizvi, I. Photochemical Targeting of Mitochondria to Overcome Chemoresistance in Ovarian Cancer. *Photochem. Photobiol.* **2023**, *99*, 448.
(14) Tedesco, A.; Rotta, J.; Lunardi, C. Synthesis, Photophysical and Photochemical Aspects of Phthalocyanines for Photodynamic Therapy. *Curr. Org. Chem.* **2005**, *7*, 187−196.
(15) Lange, C.; Bednarski, P. Photosensitizers for Photodynamic Therapy: Photochemistry in the Service of Oncology. *Curr. Pharm. Des.* **2017**, *22*, 6956−6974.
(16) Zhao, Y. Y.; Zhang, L.; Chen, Z.; Zheng, B. Y.; Ke, M.; Li, X.; Huang, J. D. Nanostructured Phthalocyanine Assemblies with Efficient Synergistic Effect of Type i Photoreaction and Photothermal Action to Overcome Tumor Hypoxia in Photodynamic Therapy. *J. Am. Chem. Soc.* **2021**, *143*, 13980−13989.
(17) Arora, A.; Singh, K. Click Chemistry Mediated by Photochemical Energy. *ChemistrySelect* **2022**, *7*, No. e202200541.
(18) Kasha, M. Characterization of electronic transitions in complex molecules. *Discuss. Faraday Soc.* **1950**, *9*, 14−19.
(19) Lewis, G. N.; Kasha, M. Phosphorescence and the Triplet State. *J. Am. Chem. Soc.* **1944**, *66*, 2100−2116.
(20) Jhun, B. H.; Jeong, D. Y.; Nah, S.; Park, S. Y.; You, Y. Novel anti-Kasha fluorophores exhibiting dual emission with thermally activated delayed fluorescence through detouring triplet manifolds. *Journal of Materials Chemistry C* **2021**, *9*, 7083−7093.
(21) Röhrs, M.; Escudero, D. Multiple Anti-Kasha Emissions in Transition-Metal Complexes. *J. Phys. Chem. Lett.* **2019**, *10*, 5798−5804.
(22) Turro, N. J.; Ramamurthy, V.; Scaiano, J. C. *Quantum Yields for Emission*; University Science Books, 2009; p 518.
(23) Schatz, G. C.; Ratner, M. A. *Quantum mechanics in chemistry*; Dover Publications, 2002; p 361.
(24) Gritsan, N. P.; Gudmundsdóttir, A. D.; Tigelaar, D.; Zhu, Z.; Karney, W. L.; Hadad, C. M.; Platz, M. S. A laser flash photolysis and quantum chemical study of the fluorinated derivatives of singlet phenylnitrene. *J. Am. Chem. Soc.* **2001**, *123*, 1951−1962.
(25) Caldwell, R. A. In *Kinetics and Spectroscopy of Carbenes and Biradicals*; Platz, M. S., Ed.; Springer: Boston, MA, 1990; pp 77−116.
(26) Valeur, B.; Berberan-Santos, M. N. *Molecular Fluorescence: Principles and Applications*, 2nd ed.; Wiley-VCH GmbH, 2012.
(27) Castro Junior, J. G. M.; Rocha, W. R. Theoretical investigation of [Ru(bpy)2(HAT)]2+ (HAT = 1,4,5,8,9,12-hexaazatriphenylene; bpy = 2,2'-bipyridine): Photophysics and reactions in excited state. *Spectrochimica Acta Part A: Molecular and Biomolecular Spectroscopy* **2022**, *270*, 120817.
(28) Yoshinaga, M.; Rocha, W. R. Theoretical Investigation of the 4,5-Dibromorodamine Methyl Ester (TH9402) Photosensitizer Used in Photodynamic Therapy: Photophysics, Reactions in the Excited State, and Interactions with DNA. *J. Phys. Chem. B* **2021**, *125*, 8932−8943.
(29) Tatchen, J.; Gilka, N.; Marian, C. M. Intersystem crossing driven by vibronic spin−orbit coupling: a case study on psoralen. *Phys. Chem. Chem. Phys.* **2007**, *9*, 5209−5221.
(30) Marian, C. M.; Föller, J.; Kleinschmidt, M.; Etinski, M. In *Intersystem Crossing Processes in TADF Emitters*; Yersin, H., Ed.; John Wiley & Sons, Ltd, 2018; pp 257−296.
(31) Shizu, K.; Kaji, H. Theoretical Determination of Rate Constants from Excited States: Application to Benzophenone. *J. Phys. Chem. A* **2021**, *125*, 9000−9010.
(32) Nakajima, T.; Kato, S. An ab initio study of the internal conversion rate from the first singlet excited state to the ground state in formaldehyde. *J. Chem. Phys.* **1996**, *105*, 5927.
(33) Miyazaki, K.; Ananth, N. Singularity-free internal conversion golden-rule rate with application to correlated triplet pair recombination in bipentacenes. *J. Chem. Phys.* **2022**, *156*, 044111.
(34) Shi, L.; Xie, X.; Troisi, A. Rapid calculation of internal conversion and intersystem crossing rate for organic materials discovery. *J. Chem. Phys.* **2022**, *157*, 134106.
(35) Lin, Z.; Kohn, A. W.; Van Voorhis, T. Toward Prediction of Nonradiative Decay Pathways in Organic Compounds II: Two Internal Conversion Channels in BODIPYs. *J. Phys. Chem. C* **2020**, *124*, 3925−3938.
(36) Kohn, A. W.; Lin, Z.; Van Voorhis, T. Toward Prediction of Nonradiative Decay Pathways in Organic Compounds I: The Case of Naphthalene Quantum Yields. *J. Phys. Chem. C* **2019**, *123*, 15394−15402.
(37) Fumanal, M.; Plasser, F.; Mai, S.; Daniel, C.; Gindensperger, E. Interstate vibronic coupling constants between electronic excited states for complex molecules. *J. Chem. Phys.* **2018**, *148*, 124119.
(38) Zobel, J. P.; Knoll, T.; González, L. Ultrafast and long-time excited state kinetics of an NIR-emissive vanadium(III) complex II.

Elucidating triplet-to-singlet excited-state dynamics. *Chemical Science* **2021**, *12*, 10791−10801.
(39) Ulstrup, J.; Jortner, J. The effect of intramolecular quantum modes on free energy relationships for electron transfer reactions. *J. Chem. Phys.* **1975**, *63*, 4358−4368.
(40) Marcus, R. A. On the theory of oxidation-reduction reactions involving electron transfer. I. *J. Chem. Phys.* **1956**, *24*, 966−978.
(41) Marcus, R. A. Nonadiabatic processes involving quantum-like and classical-like coordinates with applications to nonadiabatic electron transfers. *J. Chem. Phys.* **1984**, *81*, 4494.
(42) Marcus, R. A. Electron transfer reactions in chemistry. Theory and experiment. *Rev. Mod. Phys.* **1993**, *65*, 599.
(43) Marcus, R. A. Electrostatic Free Energy and Other Properties of States Having Nonequilibrium Polarization. I. *J. Chem. Phys.* **1956**, *24*, 979.
(44) Brédas, J. L.; Beljonne, D.; Coropceanu, V.; Cornil, J. Charge-transfer and energy-transfer processes in π-conjugated oligomers and polymers: A molecular picture. *Chem. Rev.* **2004**, *104*, 4971−5003.
(45) Chaudhuri, S.; Hedstrom, S.; Mendez-Hernandez, D. D.; Hendrickson, H. P.; Jung, K. A.; Ho, J.; Batista, V. S. Electron Transfer Assisted by Vibronic Coupling from Multiple Modes. *J. Chem. Theory Comput.* **2017**, *13*, 38.
(46) Turró, C.; Zaleski, J. M.; Karabatsos, Y. M.; Nocera, D. G. Bimolecular electron transfer in the Marcus inverted region. *J. Am. Chem. Soc.* **1996**, *118*, 6060−6067.
(47) Dirac, P. A. M. The quantum theory of the emission and absorption of radiation. *Proceedings of the Royal Society of London. Series A, Containing Papers of a Mathematical and Physical Character* **1927**, *114*, 243−265.
(48) Huang, K. Lattice relaxation and multiphonon transitions. *Contemporary Physics* **1981**, *22*, 599−612.
(49) Reimers, J. R. A practical method for the use of curvilinear coordinates in calculations of normal-mode-projected displacements and Duschinsky rotation matrices for large molecules. *J. Chem. Phys.* **2001**, *115*, 9103.
(50) Fornari, R. P.; Aragó, J.; Troisi, A. A very general rate expression for charge hopping in semiconducting polymers. *J. Chem. Phys.* **2015**, *142*, 184105.
(51) Das, A.; Kamatham, N.; Raj, A. M.; Sen, P.; Ramamurthy, V. Marcus Relationship Maintained during Ultrafast Electron Transfer across a Supramolecular Capsular Wall. *J. Phys. Chem. A* **2020**, *124*, 5297−5305.
(52) Hershberger, J. W.; Klingler, R. J.; Kochi, J. K. Electron-Transfer Catalysis. Radical Chain Mechanism for the Ligand Substitution of Metal Carbonyls. *J. Am. Chem. Soc.* **1982**, *104*, 3034−3043.
(53) Holzwarth, A. R.; Müller, M. G.; Reus, M.; Nowaczyk, M.; Sander, J.; Rögner, M. Kinetics and mechanism of electron transfer in intact photosystem II and in the isolated reaction center: Pheophytin is the primary electron acceptor. *Proc. Natl. Acad. Sci. U.S.A.* **2006**, *103*, 6895−6900.
(54) Osyczka, A.; Moser, C. C.; Daldal, F.; Dutton, P. L. Reversible redox energy coupling in electron transfer chains. *Nature* **2004**, *427*, 607−612.
(55) Closs, G. L.; Calcaterra, L. T.; Green, N. J.; Penfield, K. W.; Miller, J. R. Distance, stereoelectronic effects, and the marcus inverted region in intramolecular electron transfer in organic radical anions. *J. Phys. Chem.* **1986**, *90*, 3673−3683.
(56) Miller, J. R.; Calcaterra, L. T.; Closs, G. L. Intramolecular Long-Distance Electron Transfer in Radical Anions. The Effects of Free Energy and Solvent on the Reaction Rates. *J. Am. Chem. Soc.* **1984**, *106*, 3047−3049.
(57) Burquel, A.; Lemaur, V.; Beljonne, D.; Lazzaroni, R.; Cornil, J. Pathways for photoinduced charge separation and recombination at donor-acceptor heterojunctions: The case of oligophenylenevinylene-perylene bisimide complexes. *J. Phys. Chem. A* **2006**, *110*, 3447−3453.
(58) Geng, Y.; Wang, J.; Wu, S.; Li, H.; Yu, F.; Yang, G.; Gao, H.; Su, Z. Theoretical discussions on electron transport properties of perylene bisimide derivatives with different molecular packings and intermolecular interactions. *J. Mater. Chem.* **2011**, *21*, 134−143.
(59) Di Donato, E.; Fornari, R. P.; Di Motta, S.; Li, Y.; Wang, Z.; Negri, F. N-type charge transport and mobility of fluorinated perylene bisimide semiconductors. *J. Phys. Chem. B* **2010**, *114*, 5327−5334.
(60) Beckett, A.; Porter, G. Primary photochemical processes in aromatic molecules. Part 9.—Photochemistry of benzophenone in solution. *Trans. Faraday Soc.* **1963**, *59*, 2038−2050.
(61) Gillispie, G. D.; Lim, E. C. Further results on the triplet-triplet fluorescence of anthracenes. *Chem. Phys. Lett.* **1979**, *63*, 355−359.
(62) Tittelbach-Helmrich, D.; Steer, R. P. Measurements of the subpicosecond relaxation rates of the first excited singlet states of some pseudoazulenes in solution. *Chem. Phys.* **1995**, *197*, 99−106.
(63) Valiev, R. R.; Cherepanov, V. N.; Baryshnikov, G. V.; Sundholm, D. First-principles method for calculating the rate constants of internal-conversion and intersystem-crossing transitions. *Phys. Chem. Chem. Phys.* **2018**, *20*, 6121−6133.
(64) Suzuki, K.; Demeter, A.; Kühnle, W.; Tauer, E.; Zachariasse, K. A.; Tobita, S.; Shizuka, H. Internal conversion in 4-substituted 1-naphthylamines. Influence of the electron donor/acceptor substituent character. *Phys. Chem. Chem. Phys.* **2000**, *2*, 981−991.
(65) Sun, H.; Hoffman, M. Z. Photophysics of Ru(II)-diimine complexes in H2O-CH3CN mixed solvents. *J. Phys. Chem.* **1993**, *97*, 11956−11959.
(66) Neese, F.; Wiley, J. The ORCA program system. *Wiley Interdisciplinary Reviews: Computational Molecular Science* **2012**, *2*, 73−78.
(67) Neese, F. Software update: The ORCA program system—Version 5.0. *Wiley Interdisciplinary Reviews: Computational Molecular Science* **2022**, *12*, No. e1606.
(68) Lee, C.; Yang, W.; Parr, R. G. Development of the Colle-Salvetti correlation-energy formula into a functional of the electron density. *Phys. Rev. B* **1988**, *37*, 785.
(69) Weigend, F.; Ahlrichs, R. Balanced basis sets of split valence, triple zeta valence and quadruple zeta valence quality for H to Rn: Design and assessment of accuracy. *Phys. Chem. Chem. Phys.* **2005**, *7*, 3297−3305.
(70) Grimme, S.; Antony, J.; Ehrlich, S.; Krieg, H. A consistent and accurate ab initio parametrization of density functional dispersion correction (DFT-D) for the 94 elements H-Pu. *J. Chem. Phys.* **2010**, *132*, 154104.
(71) Grimme, S.; Ehrlich, S.; Goerigk, L. Effect of the damping function in dispersion corrected density functional theory. *J. Comput. Chem.* **2011**, *32*, 1456−1465.
(72) Neese, F. An improvement of the resolution of the identity approximation for the formation of the Coulomb matrix. *J. Comput. Chem.* **2003**, *24*, 1740−1747.
(73) Weigend, F. Accurate Coulomb-fitting basis sets for H to Rn. *Phys. Chem. Chem. Phys.* **2006**, *8*, 1057−1065.
(74) Hirata, S.; Head-Gordon, M. Time-dependent density functional theory within the Tamm−Dancoff approximation. *Chem. Phys. Lett.* **1999**, *314*, 291−299.
(75) Cossi, M.; Rega, N.; Scalmani, G.; Barone, V. Energies, structures, and electronic properties of molecules in solution with the C-PCM solvation model. *J. Comput. Chem.* **2003**, *24*, 669−681.
(76) Cammi, R.; Mennucci, B.; Tomasi, J. Fast Evaluation of Geometries and Properties of Excited Molecules in Solution: A Tamm-Dancoff Model with Application to 4-Dimethylaminobenzonitrile. *J. Phys. Chem. A* **2000**, *104*, 5631−5637.
(77) Robinson, G. W.; Frosch, R. P. Electronic Excitation Transfer and Relaxation. *J. Chem. Phys.* **1963**, *38*, 1187.
(78) Wu, Q.; Van Voorhis, T. Direct calculation of electron transfer parameters through constrained density functional theory. *J. Phys. Chem. A* **2006**, *110*, 9212−9218.
(79) López-Estrada, O.; Laguna, H. G.; Barrueta-Flores, C.; Amador-Bedolla, C. Reassessment of the Four-Point Approach to the Electron-Transfer Marcus-Hush Theory. *ACS Omega* **2018**, *3*, 2130−2140.
(80) Lawetz, V.; Orlandi, G.; Siebrand, W.; Siebrand, W. Theory of Intersystem Crossing in Aromatic Hydrocarbons. *J. Chem. Phys.* **1972**, *56*, 4058.

https://doi.org/10.1021/acs.jctc.2c01288
J. Chem. Theory Comput. 2023, 19, 2316−2326

(81) Shao, Y.; Head-Gordon, M.; Krylov, A. I. The spin−flip approach within time-dependent density functional theory: Theory and applications to diradicals. *J. Chem. Phys.* **2003**, *118*, 4807.
(82) Maeda, S.; Ohno, K.; Morokuma, K. Updated branching plane for finding conical intersections without coupling derivative vectors. *J. Chem. Theory Comput.* **2010**, *6*, 1538−1545.
(83) Send, R.; Furche, F. First-order nonadiabatic couplings from time-dependent hybrid density functional response theory: Consistent formalism, implementation, and performance. *J. Chem. Phys.* **2010**, *132*, 044107.
(84) Hay, P. J.; Wadt, W. R. Ab initio effective core potentials for molecular calculations. Potentials for K to Au including the outermost core orbitals. *J. Chem. Phys.* **1985**, *82*, 299.
(85) Frisch, M. J.; Trucks, G. W.; Schlegel, H. B.; Scuseria, G. E.; Robb, M. A.; Cheeseman, J. R.; Scalmani, G.; Barone, V.; Mennucci, B.; Petersson, G. A.; Nakatsuji, H.; Caricato, M.; Li, X.; Hratchian, H. P.; Izmaylov, A. F.; Bloino, J.; Zheng, G.; Sonnenberg, J. L.; Hada, M.; Ehara, M.; Toyota, K.; Fukuda, R.; Hasegawa, J.; Ishida, M.; Nakajima, T.; Honda, Y.; Kitao, O.; Nakai, H.; Vreven, T.; Montgomery, J. A., Jr.; Peralta, J. E.; Ogliaro, F.; Bearpark, M.; Heyd, J. J.; Brothers, E.; Kudin, K. N.; Staroverov, V. N.; Kobayashi, R.; Normand, J.; Raghavachari, K.; Rendell, A.; Burant, J. C.; Iyengar, S. S.; Tomasi, J.; Cossi, M.; Rega, N.; Millam, J. M.; Klene, M.; Knox, J. E.; Cross, J. B.; Bakken, V.; Adamo, C.; Jaramillo, J.; Gomperts, R.; Stratmann, R. E.; Yazyev, O.; Austin, A. J.; Cammi, R.; Pomelli, C.; Ochterski, J. W.; Martin, R. L.; Morokuma, K.; Zakrzewski, V. G.; Voth, G. A.; Salvador, P.; Dannenberg, J. J.; Dapprich, S.; Daniels, A. D.; Farkas, O.; Foresman, J. B.; Ortiz, J. V.; Cioslowski, J.; Fox, D. J. *Gaussian-09*, rev. E.01; Gaussian Inc.: Wallingford CT, 2009.
(86) Humeniuk, A.; Bužančić, M.; Hoche, J.; Cerezo, J.; Mitrić, R.; Santoro, F.; Bonačić-Koutecký, V. Predicting fluorescence quantum yields for molecules in solution: A critical assessment of the harmonic approximation and the choice of the lineshape function. *J. Chem. Phys.* **2020**, *152*, 054107.
(87) Valiev, R. R.; Cherepanov, V. N.; Nasibullin, R. T.; Sundholm, D.; Kurten, T. Calculating rate constants for intersystem crossing and internal conversion in the Franck−Condon and Herzberg−Teller approximations. *Phys. Chem. Chem. Phys.* **2019**, *21*, 18495−18500.
(88) Valiev, R. R.; Nasibullin, R. T.; Cherepanov, V. N.; Kurtsevich, A.; Sundholm, D.; Kurtén, T. Fast estimation of the internal conversion rate constant in photophysical applications. *Phys. Chem. Chem. Phys.* **2021**, *23*, 6344−6348.
(89) Nijegorodov, N.; Ramachandran, V.; Winkoun, D. P. The dependence of the absorption and fluorescence parameters, the intersystem crossing and internal conversion rate constants on the number of rings in polyacene molecules. *Spectrochimica Acta - Part A: Molecular and Biomolecular Spectroscopy* **1997**, *53*, 1813−1824.
(90) Marazzi, M.; Mai, S.; Roca-Sanjuán, D.; Delcey, M. G.; Lindh, R.; González, L.; Monari, A. Benzophenone Ultrafast Triplet Population: Revisiting the Kinetic Model by Surface-Hopping Dynamics. *J. Phys. Chem. Lett.* **2016**, *7*, 622−626.
(91) Bryantseva, N. G.; Sokolova, I. V.; Gadirov, R. M.; Khilya, V. P.; Garazd, Y. L. Luminescence characteristics of new substituted coumarins. *J. Appl. Spectrosc.* **2009**, *76*, 813−818.
(92) Szaciłowski, K.; Macyk, W.; Drzewiecka-Matuszek, A.; Brindell, M.; Stochel, G. Bioinorganic photochemistry: Frontiers and mechanisms. *Chem. Rev.* **2005**, *105*, 2647−2694.

https://doi.org/10.1021/acs.jctc.2c01288
J. Chem. Theory Comput. 2023, 19, 2316−2326